Crossover from Spin-Flop Coupling to Collinear Spin Alignment in Antiferromagnetic/Ferromagnetic Nanostructures

ARTICLE *in* NANO LETTERS · APRIL 2012

Impact Factor: 13.59 · DOI: 10.1021/nl300361e · Source: PubMed

NANO LETTERS

Letter

pubs.acs.org/NanoLett

Crossover from Spin-Flop Coupling to Collinear Spin Alignment in Antiferromagnetic/Ferromagnetic Nanostructures

Erik Folven,*[,†] Andreas Scholl,[‡] Anthony Young,[‡] Scott T. Retterer,[§] Jos E. Boschker,[†] Thomas Tybell,[†] Yayoi Takamura,[⊥] and Jostein K. Grepstad[†]

[†]Department of Electronics and Telecommunications, Norwegian University of Science and Technology, NO-7491 Trondheim, Norway

[‡]Advanced Light Source, Lawrence Berkeley National Laboratory, Berkeley, California 94720, United States

[§]Oak Ridge National Laboratory, P.O. Box 2008 MS 6123, Oak Ridge, Tennessee 37831, United States

[⊥]Department of Chemical Engineering and Materials Science, University of California—Davis, Davis, California 95616, United States

ABSTRACT: The technologically important exchange coupling in antiferromagnetic/ferromagnetic bilayers is investigated for embedded nanostructures defined in a $LaFeO_3/La_{0.7}Sr_{0.3}MnO_3$ bilayer. Exploiting the element specificity of soft X-ray spectromicroscopy, we selectively probe the magnetic order in the two layers. A transition from perpendicular to parallel spin alignment is observed for these nanostructures, dependent on size and crystalline orientation. The results show that shape-induced anisotropy in the antiferromagnet can override the interface exchange coupling in spin-flop coupled nanostructures.

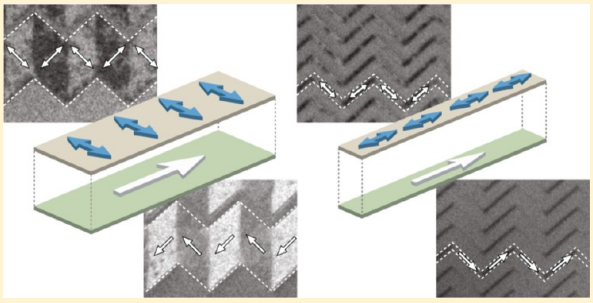

KEYWORDS: *Spin-flop coupling, size effects, embedded nanostructures, magnetic dichroism, X-PEEM*

Perovskite oxides with the chemical formula ABO_3 display a wide range of technologically relevant functional properties, such as ferromagnetism, ferroelectricity, and high-T_C superconductivity. Furthermore, recent studies have shown that perovskite oxide interfaces can possess properties not found in the constituent materials.[1] Exchange bias coupling between adjacent ferromagnetic (FM) and antiferromagnetic (AFM) layers shifts the hysteresis loop by an amount $\mathbf{H}_{eb}$ along the magnetic field axis, and this effect is vital to commercial devices such as magnetic recording read heads, random access memory, and magnetic sensors.[2] Different models have been proposed to describe exchange bias,[3−7] involving parameters such as uncompensated spins in the AFM layer and domain walls in the FM and AFM layers. However, for an atomically smooth interface between a ferromagnet and a fully compensated AFM layer, such as the (001)-plane of a G-type antiferromagnet, there is an equal number of positive and negative exchange interactions. A microscopic Heisenberg model shows that for such compensated interfaces a perpendicular alignment of the FM and AFM spins is energetically favorable.[6,8] An increased uniaxial anisotropy in the FM layer is predicted to result from this coupling, giving rise to increased coercivity, but no unidirectional shift of the FM hysteresis loop, i.e., no exchange bias.[9]

Experimental evidence of perpendicular spin coupling in FM/AFM systems, commonly referred to as *spin-flop coupling*, has been reported using neutron diffraction,[10] from the shape of the magnetic hysteresis loops,[11,12] using soft X-ray absorption spectroscopy[13] and by photoemission electron microscopy (X-PEEM).[14] More recently, X-PEEM was used to directly image the ferromagnetic (FM) and antiferromagnetic (AFM) domains in $La_{0.7}Sr_{0.3}MnO_3$ (LSMO)/$La_{0.7}Sr_{0.3}FeO_3$ (LSFO) superlattices with a [6 unit cell (u.c.) LSMO][6 u.c. LSFO] repeat period.[15] In this study, Yang et al. found a close correspondence of each AFM domain with two types of smaller FM domains, so that locally the AFM spin axis is perpendicular to the magnetization of the FM layer. The locations of the correlated AFM and FM domains changed with temperature, suggesting that the spin-flop coupling is sufficiently strong to overcome the pinning effect of structural defects, which typically define the location of AFM domains.[16]

Here, we report on how size and orientation relative to the crystalline axes of nanostructures defined in epitaxial LFO/LSMO bilayers affect the spin alignment and exchange coupling at this AFM/FM interface. The element specificity of X-PEEM permits the magnetic order in the two layers to be probed individually. Furthermore, the magnetic ordering temperature (T_N) of the AFM layer exceeds that (T_C) of the FM layer. Thus, the impact from magnetic coupling between the two layers on the AFM domain structure can be examined both above and below the Curie temperature of the LSMO layer. We find that the relative orientation of the spins in the AFM and FM epilayers depends on the size of the nanostructures as well as the orientation of their edges with respect to the film

Received: January 27, 2012
Revised: March 29, 2012
Published: April 2, 2012

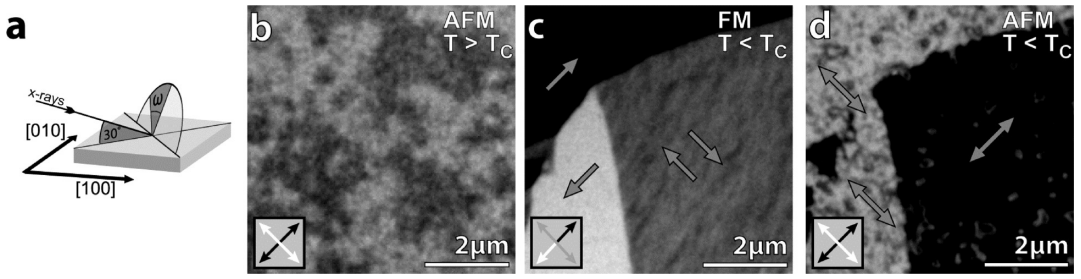

Figure 1. (a) Schematic of the measurement geometry for the X-PEEM measurements and X-PEEM images showing the (b) AFM domain structure above T_C (T = 300 K), (c) the FM domain structure below T_C (T = 100 K), and (d) the corresponding AFM domain structure below T_C (T = 100 K). The legend in the lower left corner of images b–d illustrates the X-PEEM contrast resulting from the adopted experimental geometry and choice of polarization angle (ω = 90°).

crystalline axes. A crossover from perpendicular (spin-flop) coupling to parallel alignment of the AFM and FM spins is observed upon reduction of the nanostructure dimensions. This behavior is explained in terms of a competition between shape-induced anisotropy in the antiferromagnet and the interface exchange coupling in spin-flop coupled nanostructures and offers the possibility to control spin alignment through nanostructure size and orientation.

The LFO [10 u.c.]/LSMO [90 u.c.] bilayer was grown by pulsed laser deposition on (001)-oriented Nb-doped $SrTiO_3$ (Nb:STO (0.05 wt % Nb)) substrate (for details, see ref 17). The surface topography of the as-grown sample was investigated by atomic force microscopy. A step-and-terrace surface morphology of the 0.1° miscut Nb:STO substrate was found to be preserved for the bilayer films. High-resolution X-ray diffraction measurements confirm coherent growth and films of high crystalline quality. The out-of-plane lattice constants were determined to be $(d_{001})_{pc}$ = 4.04 Å for the LFO layer and $(d_{001})_{pc}$ = 3.85 Å for LSMO (pc = pseudocubic notation). The LSMO Curie temperature was assessed from superconducting quantum interference device (SQUID) measurements at $T_C \sim 270$ K. The nanostructures were defined in the LFO/LSMO bilayer using a patterning technique which relies on local disruption of the structural and magnetic order by Ar^+ ion implantation using a Cr hard mask (for details, see refs 18 and 19).

The FM and AFM domain patterns of the LSMO and LFO layers were imaged using the PEEM-3 Microscope at the Advanced Light Source. Images with magnetic domain contrast were obtained using the polarization dependence of X-ray absorption in magnetically ordered materials, i.e., magnetic dichroism. In ferromagnetically ordered materials, X-ray absorption depends on the relative orientation of the helicity of circularly polarized X-rays and the local magnetization, i.e., X-ray magnetic circular dichroism (XMCD). The FM domain patterns displayed in this Letter were obtained by dividing X-PEEM images recorded with right- and left-handed helicity of the incident X-rays, respectively, for an energy near the Mn L_3 absorption edge in LSMO. This procedure serves to remove sources of contrast other than magnetic dichroism from the PEEM images, such as topographic or work function contrast. For an antiferromagnet, the X-ray absorption depends on the relative orientation of the **E**-vector of linearly polarized X-rays and the AFM spin axes, i.e., X-ray magnetic linear dichroism (XMLD). The AFM domain images were obtained likewise, by division of PEEM images recorded at two different photon energies.[20] Here, we take advantage of the large XMLD at the Fe L_2-edge of LFO.[21] The experimental geometry for the XMLD- and XMCD-PEEM measurements is depicted in Figure 1a. The X-rays were incident on the sample surface at an angle of 30°, with their projection along the [110] crystalline axis of the Nb:STO substrate. In the PEEM-3 microscope, the polarization plane for linearly polarized X-rays can be rotated from ω = 0° (i.e., the **E**-vector in the plane of incidence) to ω = 90° (i.e., the **E**-vector in the plane of the sample surface). Maximum domain contrast for AFM domains is obtained for the AFM spin axis oriented parallel and perpendicular to the **E**-vector, respectively. With the experimental geometry shown in Figure 1a, the preferred choice of ω for imaging of domains with their AFM spin axis oriented along in-plane ⟨110⟩ and ⟨100⟩ directions is ω = 90° and ω = 45°, respectively.

Figure 1b depicts the spontaneous AFM domain structure in the LFO layer, as obtained by XMLD-PEEM at room temperature, i.e., above T_C of the LSMO layer, with a polarization angle ω = 90°. The analysis required to determine the AFM spin orientation from the measured X-PEEM contrast is discussed in previous reports.[19,22] When cooling the sample below T_C, a FM domain structure forms in the LSMO layer. The XMCD-PEEM image acquired at 100 K (Figure 1c) displays a region where three distinct FM domains intersect. These domains show black, white, and gray contrast corresponding to magnetic moments oriented parallel, antiparallel, and perpendicular to the helical orientation of the circularly polarized X-rays, respectively; i.e., the magnetic moments are oriented along the in-plane ⟨110⟩ easy axes of the LSMO layer under tensile strain.[23] The associated AFM domain structure in the LFO layer, recorded at 100 K with ω = 90°, is shown in Figure 1d. We note the close correspondence with the domains in the LSMO layer. Domains with gray contrast in Figure 1c appear predominantly black in the AFM domain image, whereas domains with black or white contrast in Figure 1c appear mainly white in the AFM domain image. Observing the contrast arising from different spin orientations in the actual experimental geometry, these images confirm a spin-flop coupling with perpendicular orientation of the AFM spin axis and the FM magnetization. This implies that locally the AFM spin axis is rotated up to 90° relative to its orientation above T_C. The spontaneous domain structure in an antiferromagnet is commonly attributed to crystalline imperfections and twin boundaries.[16] The speckle observed within the large AFM domains in Figure 1d is attributed to domain wall pinning centers in the LFO layer, sufficiently strong to resist rotation of the associated spins by coupling to the FM layer as the system is cooled below T_C.

In order to explore the impact on the spin axis alignment from shape, size, and orientation of nanostructures, we define

dx.doi.org/10.1021/nl300361e | Nano Lett. 2012, 12, 2386–2390

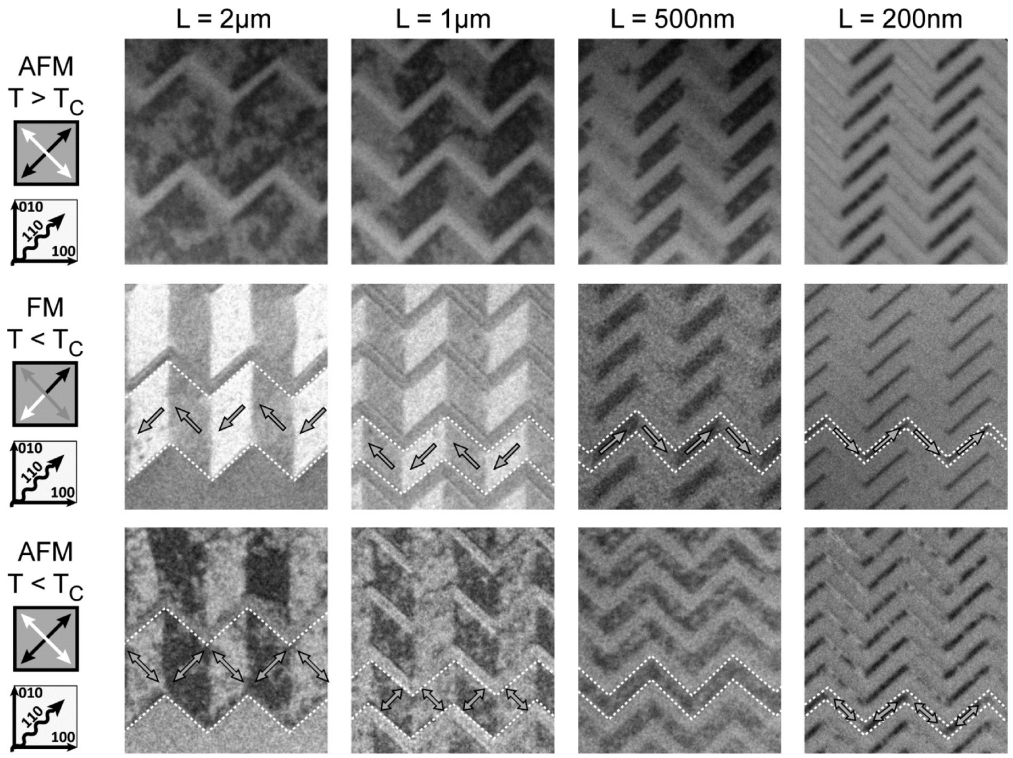

Figure 2. X-PEEM images of nanowires with their edges aligned with the in-plane ⟨110⟩ directions. The micrographs show the AFM domain patterns in LFO at T = 300 K (above T_C, top row), the FM domain patterns in LSMO at T = 100 K (below T_C, middle row), and the corresponding AFM domain pattern in LFO at 100 K (below T_C, bottom row). The experimental geometry and resulting X-PEEM contrast are illustrated in the schematics on the left.

zigzag line patterns in the AFM/FM bilayer. By keeping the length of the straight segments fixed and defining patterns with line widths ranging from 2 μm to 200 nm, the aspect ratio of the individual segments is effectively changed by a factor 10. Nanowires with this particular geometry allow for investigation of two orthogonal directions in the same measurement. Patterns were defined with their edges oriented parallel to in-plane ⟨110⟩ and ⟨100⟩ directions corresponding to the magnetic easy and hard directions of LSMO under tensile strain,[23] respectively. We have recently reported the in-plane <110> and <100> directions to be the AFM easy axis directions for LFO grown on LSMO.[17] Figure 2 shows XMLD- and XMCD-PEEM images for zigzag line patterns of varying width, defined with their edges parallel to the in-plane ⟨110⟩ axes. The XMLD-PEEM images were obtained using an X-ray polarization angle of ω = 90°, thus maximizing the sensitivity for AFM domains with their spins aligned parallel to the edges. As recently reported,[17,19] nanostructure edges defined along easy directions in LFO promote the formation of extended AFM domains with this spin orientation. The origin of this edge-induced anisotropy is not well understood and cannot be explained in terms of long-range dipole interactions, as in the case of shape anisotropy for a ferromagnet. However, long-range magnetoelastic forces have been proposed as a source of shape-induced effects in finite-sized antiferromagnets.[24] The ion implantation process has been shown to result in swelling of the implanted matrix,[19] which could impose in-plane strain on the nanostructures. For the 2 μm wide lines, the formation of such extended domains at room temperature is restricted to a narrow zone close to the edges. As the line width decreases, the stabilized domains at opposite edges move closer and eventually overlap. For line widths of 500 nm or less, the AFM domain structure appears completely dominated by these edge-induced domains.

As the thin film bilayer is cooled below T_C of the LSMO layer, a FM domain structure governed by shape anisotropy is established in these zigzag nanowires (Figure 2, middle row). The FM domains of the 2 and 1 μm wide nanowires with alternating white and gray contrast correspond to a magnetization alternating between down-left (white) and up-left (gray) in these lines. The 500 and 200 nm wide nanowires with alternating black and gray contrast correspond to a magnetization alternating between down-right (gray) and up-right (black). Arrows indicating the predominant magnetization direction are included for one of the nanowires in each image. Neighboring zigzag lines are typically magnetized in the same direction, and the size of the regions with uniformly magnetized nanowires in Figure 2 is comparable to the individual FM domains in a blanket (LSMO) film (cf. Figure 1c). The AFM domain structure in the LFO layer (Figure 2, bottom row) changes dramatically compared to that observed above T_C, the AFM domains in the 2 and 1 μm wide zigzag lines are now strongly correlated with the magnetic domains of the underlying ferromagnet. Investigation of their spin orientations reveals a 90° spin-flop coupling, as expected from the data for an unpatterned film. This result shows that the spin axis of the edge-induced AFM domains observed at room temperature has rotated through 90° by exchange coupling to the FM layer. Unlike the situation above T_C where the shape-induced domain stabilization only persists to about 400 nm from the perimeter of the nanowires, below T_C the spin-flop coupled AFM domains extend across the full width of the nanowires, thus forming domains in the shape of a parallelogram for these zigzag line patterns.

dx.doi.org/10.1021/nl300361e | *Nano Lett.* 2012, 12, 2386−2390

For nanowires with a line width of 500 nm, the picture changes. The FM domain structure in the LSMO layer is still controlled by shape anisotropy, whereas the AFM domains of the LFO layer consist of smaller domains (~300 nm) similar to those seen in unpatterned films. The shape-induced domain stabilization, which governs the domain configuration at room temperature, is now absent, and there is no visible correlation with the FM domains in LSMO. For line widths of 200 nm, however, the AFM spins in these elongated domains are all aligned with the nanowire edges, similar to the AFM domain configuration above T_C, and parallel to the spins of the FM domains in the LSMO layer. Hence, the AFM and FM spins are collinear for these 200 nm wide bilayer nanowires. This finding suggests that the exchange coupling of AFM and FM domains in these narrow nanowires is no longer strong enough to reorient the AFM spins perpendicular to the magnetization of the FM domains. As a consequence, the AFM domain structure remains in a state similar to that above T_C, dominated by edge-induced domain stabilization.

Figure 3 depicts zigzag nanowires with their edges aligned parallel to the in-plane ⟨100⟩ crystalline axes. The AFM domain

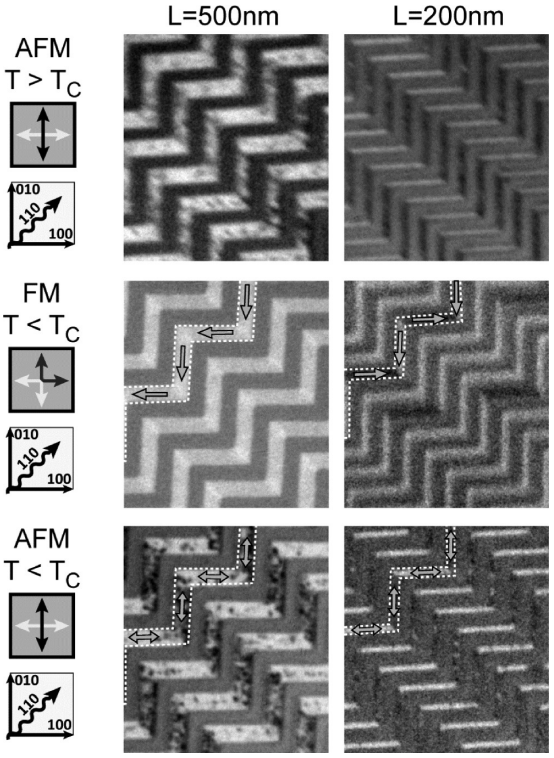

Figure 3. X-PEEM images of 500 and 200 nm wide zigzag nanowires with their edges oriented along in-plane ⟨100⟩ directions, showing AFM domain contrast at T = 300 K (above T_C, top row), FM domain contrast at T = 100 K (below T_C, middle row), and the corresponding AFM domain structure at T = 100 K (below T_C, bottom row). The experimental geometry and resulting X-PEEM contrast are illustrated in the schematics to the left.

structure above T_C is probed by XMLD-PEEM with a polarization angle ω = 40° (Figure 3, top row). For both 500 and 200 nm wide zigzag lines, extended AFM domains are seen to be stabilized along the nanowire edges above T_C. The FM domain contrast observed in the XMCD-PEEM images recorded below T_C (Figure 3, middle row) is consistent with a spin configuration governed by shape anisotropy; i.e., the spins are all aligned with the edges. The XMCD-PEEM images of the 200 and 500 nm wide nanowires in Figure 3 suggest that the magnetization of these nanowires alternate between the $[\bar{1}00]$ and $[0\bar{1}0]$ directions. A slightly brighter region can be recognized at the corners of the 500 nm wide lines, suggesting a $[\bar{1}10]$ spin direction intermediate between that of the two straight sections. The AFM domain structure below T_C is shown in Figure 3, bottom row. For the 200 nm wide lines, we observe the same collinear alignment of the magnetic moments in the AFM and FM layers as for the nanowires oriented along in-plane ⟨110⟩ axes of the Nb:STO substrate. However, for these ⟨100⟩-oriented nanostructures this collinear alignment persists also in the 500 nm wide lines.

For zigzag nanowires with a line width of 1 μm (Figure 4), the FM domains are no longer confined to the in-plane ⟨100⟩

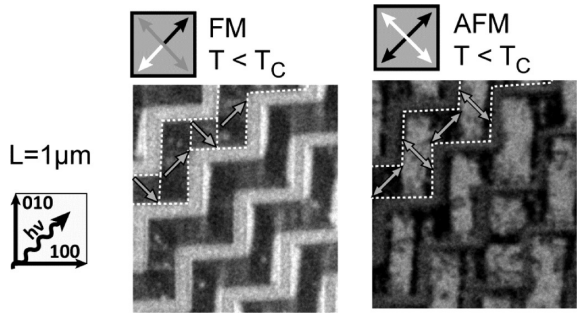

Figure 4. X-PEEM images of 1 μm wide zigzag nanowires with their edges oriented along in-plane ⟨100⟩ directions obtained at T = 100 K (below T_C), showing FM (left) and AFM (right) domain contrast. The experimental geometry and X-PEEM contrast are illustrated in the schematics to the left and above the X-PEEM images, respectively.

directions by force of shape anisotropy. These nanowires feature FM domains oriented chiefly along the in-plane ⟨110⟩ directions, i.e., the *easy directions* for LSMO films under tensile strain. Imaging the AFM domains with a polarization angle of ω = 90° reveals that the AFM domain configuration is again governed by a 90° spin-flop coupling to the ⟨110⟩-oriented FM domains, as for the case of a blanket film.

The fact that the collinear alignment of the spins in the AFM and FM layers persists to line widths exceeding 500 nm, when the nanostructures are oriented with their edges along ⟨100⟩ directions, as compared to 200 nm for nanostructures oriented along ⟨110⟩ directions, suggests that a higher energy is required for reorientation of AFM domains with their spins aligned with in-plane ⟨100⟩ crystalline directions. This is consistent with data obtained for the LFO/LSMO bilayer above the LSMO Curie temperature,[17] which show a stronger XMLD signal for ⟨100⟩-oriented domains compared to that measured for ⟨110⟩-oriented domains. A schematic summarizing the present results measured above and below T_C is shown in Figure 5.

In conclusion, we have investigated the AFM/FM interface exchange coupling for embedded nanostructures defined in an epitaxial LFO/LSMO bilayer. For a blanket film and nanostructures with dimensions exceeding ~1 μm, the interface exchange coupling favors perpendicular alignment of the spins in the respective AFM and FM layers. However, for nanostructures smaller than some critical dimension we demonstrate that edge-induced stabilization of the AFM domains will override the interface coupling, resulting in a collinear alignment of the AFM and FM spins. The possibility to use shape and crystalline orientation of embedded

dx.doi.org/10.1021/nl300361e | *Nano Lett.* 2012, 12, 2386–2390

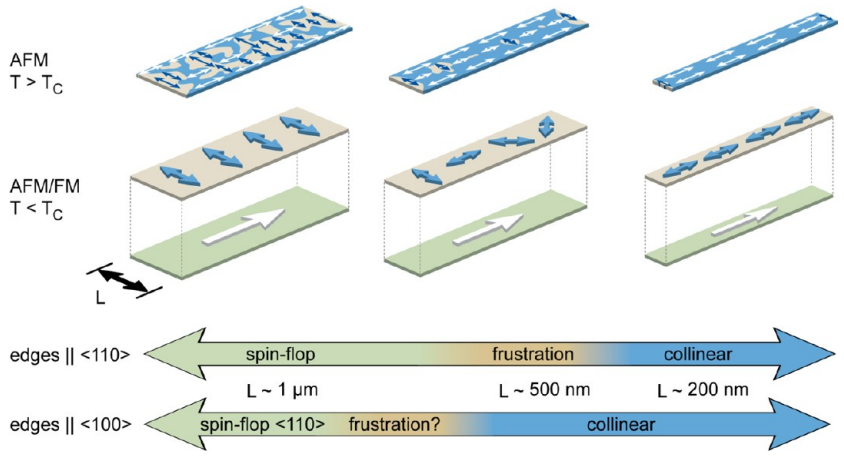

Figure 5. Schematic summarizing the domain configurations and spin alignment observed above and below T_C for embedded nanostructures in LFO/LSMO bilayers.

nanostructures to control the effective spin alignment in AFM/FM bilayers should facilitate fabrication of model systems that can shed light on the nature and strength of the magnetic coupling between an antiferromagnet and an adjacent ferromagnet. A more complete understanding of the macroscopic exchange coupling phenomena, such as increased coercivity and hysteresis loop shifts, may be obtained from measurements of magnetic switching in nanostructures with a tailored spin alignment.

AUTHOR INFORMATION

Corresponding Author

*E-mail: folven@ntnu.no.

Notes

The authors declare no competing financial interest.

ACKNOWLEDGMENTS

The authors thank Yasuhide Nakamura for help with chemical etching of the Cr hard mask. Part of this research was carried out at the Center for Nanophase Materials Sciences, which is sponsored at Oak Ridge National Laboratory by the Office of Basic Energy Sciences, U.S. Department of Energy. The Advanced Light Source is supported by the Director, Office of Science, Office of Basic Energy Sciences, of the U.S. Department of Energy under Contract DE-AC02-05CH11231. Oak Ridge National Laboratory is managed by UT-Battelle, LLC, for the U.S. Department of Energy under Contract DE-AC05-00OR22725. Partial funding for these experiments was obtained from the Norwegian Research Council under Contracts 176656 and 190086.

REFERENCES

(1) Zubko, P.; Gariglio, S.; Gabay, M.; Ghosez, P.; Triscone, J.-M. *Annu. Rev. Condens. Matter Phys.* **2011**, *2*, 141−165.
(2) Nogues, J.; Schuller, I. K. *J. Magn. Magn. Mater.* **1999**, *192*, 203−232.
(3) Meiklejohn, W. H. *J. Appl. Phys.* **1962**, *33*, 1328−1335.
(4) Malozemoff, A. P. *Phys. Rev. B* **1987**, *35*, 3679−3682.
(5) Mauri, D.; Siegmann, H. C.; Bagus, P. S.; Kay, E. *J. Appl. Phys.* **1987**, *62*, 3047−3049.
(6) Koon, N. C. *Phys. Rev. Lett.* **1997**, *78*, 4865.
(7) Kiwi, M.; Mejia-Lopez, J.; Portugal, R. D.; Ramirez, R. *Solid State Commun.* **2000**, *116*, 315−319.
(8) Hinchey, L. L.; Mills, D. L. *Phys. Rev. B* **1986**, *34*, 1689.
(9) Schulthess, T. C.; Butler, W. H. *Phys. Rev. Lett.* **1998**, *81*, 4516−4519.
(10) Ijiri, Y.; Borchers, J. A.; Erwin, R. W.; Lee, S.-H.; van der Zaag, P. J.; Wolf, R. M. *Phys. Rev. Lett.* **1998**, *80*, 608−611.
(11) Moran, T. J.; Nogues, J.; Lederman, D.; Schuller, I. K. *Appl. Phys. Lett.* **1998**, *72*, 617−619.
(12) Moran, T. J.; Schuller, I. K. *J. Appl. Phys.* **1996**, *79*, 5109−5111.
(13) Arenholz, E.; van der Laan, G.; Yang, F.; Kemik, N.; Biegalski, M. D.; Christen, H. M.; Takamura, Y. *Appl. Phys. Lett.* **2009**, *94*, 072503−3.
(14) Finazzi, M.; Brambilla, A.; Biagioni, P.; Graf, J.; Gweon, G. H.; Scholl, A.; Lanzara, A.; Duò, L. *Phys. Rev. Lett.* **2006**, *97*, 097202.
(15) Yang, F.; Kemik, N.; Scholl, A.; Doran, A.; Young, A. T.; Biegalski, M. D.; Christen, H. M.; Takamura, Y. *Phys. Rev. B* **2011**, *83*, 014417.
(16) Stohr, J.; Siegmann, H. C. *Magnetism: From Fundamentals to Nanoscale Dynamics*; Springer: Heidelberg, 2006.
(17) Folven, E.; Scholl, A.; Young, A.; Retterer, S. T.; Boschker, J. E.; Tybell, T.; Takamura, Y.; Grepstad, J. K. *Phys. Rev. B* **2011**, *84*, 220410(R).
(18) Takamura, Y.; Chopdekar, R. V.; Scholl, A.; Doran, A.; Liddle, J. A.; Harteneck, B.; Suzuki, Y. *Nano Lett.* **2006**, *6*, 1287−1291.
(19) Folven, E.; Tybell, T.; Scholl, A.; Young, A.; Retterer, S. T.; Takamura, Y.; Grepstad, J. K. *Nano Lett.* **2010**, *10*, 4578−4583.
(20) By convention, XMLD-PEEM ratio images were calculated as X-PEEM(L_{2B}) divided by X-PEEM(L_{2A}). Ratio images obtained at the same temperature are always presented with the same contrast settings. However, the contrast settings for images recorded at room temperature are slightly increased as compared to those obtained at 100 K to compensate for the temperature dependence of the XMLD signal.
(21) Scholl, A.; Stohr, J.; Luning, J.; Seo, J. W.; Fompeyrine, J.; Siegwart, H.; Locquet, J. P.; Nolting, F.; Anders, S.; Fullerton, E. E.; Scheinfein, M. R.; Padmore, H. A. *Science* **2000**, *287*, 1014−1016.
(22) Czekaj, S.; Nolting, F.; Heyderman, L. J.; Willmott, P. R.; van der Laan, G. *Phys. Rev. B* **2006**, *73*, 020401.
(23) Berndt, L. M.; Balbarin, V.; Suzuki, Y. *Appl. Phys. Lett.* **2000**, *77*, 2903−2905.
(24) Gomonay, H. V.; Loktev, V. M. *Phys. Rev. B* **2007**, *75*, 174439.